RSC Advances

PAPER

View Article Online
View Journal | View Issue



Cite this: *RSC Adv.*, 2014, **4**, 18460

# Pluronic F127–folic acid encapsulated nanoparticles with aggregation-induced emission characteristics for targeted cellular imaging†

Hongguang Lu,*[a] Xiaowei Zhao,[a] Wenjing Tian,*[b] Qiusheng Wang[a] and Ji Shi[a]

Received 16th February 2014
Accepted 3rd April 2014

DOI: 10.1039/c4ra01355g

www.rsc.org/advances

In this work, fluorescence amplified organic nanoparticles (NPs) are synthesized by incorporation of the hydrophobic aggregation-induced emission (AIE) fluorophores, 9,10-bis(4-butoxystyryl) anthracene (BOSA) and/or bis(4-(*N*-(2-naphthyl)phenylamino)-phenyl)fumaronitrile (NPAPF), using biocompatible Pluronic F127–folic acid adduct (F127–FA) as the encapsulation matrix. The emission spectrum of BOSA donor overlaps well with the absorption spectrum of NPAPF acceptor, resulting in a 3.0-fold amplified NPAPF emission signal *via* fluorescence resonance energy transfer (FRET). The obtained BOSA–NPAPF co-loaded F127–FA nanoparticles (NPs) show a large Stokes shift of 245 nm, high water dispersibility, and low cytotoxicity. Application of these NPs for targeted cellular imaging is successfully demonstrated using folate receptor (FR)-overexpressed MCF-7 breast cancer cells as an example. Using the F127–FA as the encapsulation matrix, the folate-functionalized AIE NPs show bright fluorescence signals and specific targeting effect for FR-overexpressed cancer cells. These studies indicate that the F127–FA encapsulated AIE NPs are efficient fluorescent probes for biological imaging.

## 1 Introduction

Fluorescence-based optical imaging plays a direct visual role for biological investigation, for example, for the understanding of biological processes, metabolism and pharmacokinetics, as well as for the diagnosis/detection of disease and cancer formation.[1] Among various fluorescence probes, inorganic semiconductor quantum dots (QDs)[2] have been extensively utilized for cellular imaging. Although QDs exhibit better photostability and large Stokes shifts as compared to organic dye molecules, they are commonly made of heavy metals and chalcogens (*e.g.*, CdSe and PbS) making them intrinsically toxic. And some of semiconductor QDs have also been demonstrated to be toxic to living organisms due to their heavy metal components.[3] In comparison to inorganic QDs, fluorescent organic nanoparticles (NPs) show synthetic versatility, low cytotoxicity, good photostability and facile surface functionalization for specific targeting, making them attractive alternatives for biomedical applications.[4] However, most of fluorescent organic NPs suffer a common problem. The fluorescent emissions from conventional organic fluorophores are often quenched at high concentrations or in aggregate state due to π–π stacking and other non-radiative pathways, which is known as aggregation-caused quenching (ACQ).[5] This ACQ effect obstructs the capability of increasing the fluorophore-doped concentration in NPs as a brighter emitter for bioimaging.

Recently, a new category of fluorophores with the opposite characteristics to the ACQ, aggregation-induced emission (AIE), has been developed.[6] AIE fluorophores are non-emissive in dilute solutions but are induced to emit intense fluorescence in aggregates. Since the first AIE fluorophores, 1-methyl-1,2,3,4,5-pentaphenylsilole, was reported by Tang's group,[7] many AIE fluorophores have been synthesized by various research groups, such as tetraphenylethene,[8] siloles,[9] distyrylanthracene,[10] cyano-substituted diarylethlen derivatives.[11] Restricted intramolecular rotation (RIR) has been suggested as the possible mechanism of the AIE phenomenon, considering that intramolecular rotations can drastically affect the radiative/non-radiative recombination processes of the excited state.[6,10a,11b] Since the AIE effect allows a higher concentration of fluorophores to be loaded in NPs, it makes the AIE NPs more emissive and stronger photobleaching resistance. So far, several strategies have been developed to fabricate AIE fluorophores based NPs for biosensing and bioimaging applications.[12] For example, Tang and Liu have demonstrated the incorporation of AIE fluorophores into a biocompatible molecule (bovine serum albumin or DSPE-PEG) and the bioimaging applications *in vitro* and *in vivo*.[12b,d,e] Furthermore, we have successfully synthesized a series AIE-fluorophore-containing random copolymers with high fluorescence quantum yields and explored their

[a]*Tianjin Key Laboratory of Organic Solar Cells and Photochemical Conversion, School of Chemistry & Chemical Engineering, Tianjin University of Technology, Tianjin 300384, P. R. China. E-mail: hglu@tjut.edu.cn*

[b]*State Key Laboratory of Supramolecular Structure and Materials, Jilin University, Changchun, 130012, P. R. China. E-mail: wjtian@jlu.edu.cn*

† Electronic supplementary information (ESI) available. See DOI: 10.1039/c4ra01355g

applications for cell imaging.[13] Compared with traditional organic fluorophores with ACQ effect, the AIE fluorogens are promising candidates in the development of next generation of fluorescent organic NPs for bioimaging applications. Hence, the design and synthesis of novel AIE fluorophores based NPs, which possess remarkable optical properties, high water dispersibility, target imaging and low cytotoxicity, are still highly desirable.

In this work, we demonstrate a generally applicable protocol to encapsulate hydrophobic AIE fluorophores into the biocompatible Pluronic F127 NPs for targeted cellular imaging and efficiently enhance the red AIE fluorophore emission through fluorescence resonance energy transfer (FRET). 9,10-Bis(4-butoxystyryl)anthracene (BOSA),[13a] a green-emitting AIE molecule, was selected as a FRET donor. Moreover, bis(4-(*N*-(2-naphthyl)phenylamino)-phenyl) fumaronitrile (NPAPF),[12a] a red AIE-emitter, was also selected as a FRET acceptor to couple with BOSA. By encapsulating both BOSA donor and NPAPF acceptor simultaneously within the NPs, a significant FRET effect is induced, which contributes to the notable increase of acceptor emission (3.0 folds). In addition, the obtained BOSA–NPAPF co-loaded F127 NPs show a large Stokes shift of 245 nm, which can be used to avoid the interference between excitation and emission light, as well as shift the emission spectrum away from the sample autofluorescence to result in high detection sensitivity. The targeted cellular imaging and cytotoxicity studies are successfully demonstrated using FR-overexpressed MCF-7 breast cancer cells as an example. Using the Pluronic F127–folic acid adduct (F127–FA) as the encapsulation matrix, the folate-functionalized AIE NPs show bright fluorescence signals, low cytotoxicity and specific targeting effect for FR-overexpressed cancer cells. These results indicate that the F127–FA encapsulated AIE NPs can serve as efficient fluorescent probes for biological imaging.

# 2 Experimental methods

## 2.1 Materials and instruments

All chemicals and solvents were in analytical grade and were used without further purification. BOSA[13a] and NPAPF[12a] were synthesized according to the literature. Pluronic F127 (F127), 3-(4,5-dimethyl thiazol-2-yl)-2,5-diphenyl tetrazolium bromide (MTT), fetal bovine serum (FBS) and folate-free Dulbecco's Modified Eagle's Medium (DMEM) were commercially available from Sigma-Aldrich. Folic acid (FA) and 1,1′-carbonyldiimidazole (CDI) were purchased from TCI. UV-vis spectra were recorded on a Shimadzu UV-3390 spectrophotometer. Fluorescence measurements were carried out with a Hitachi F4500 spectrofluorophotometer. Dynamic light scattering (DLS) measurements were performed using a Malvern Nano-ZS instrument at room temperature. Transmission electron microscopy (TEM) images were obtained with a transmission electron microscope (JEM-2010HR, JEOL Ltd.).

## 2.2 Synthesis of Pluronic F127–folic acid adduct (F127–FA)

F127–FA was synthesized following the literature procedure.[14b] 87.58 mg (0.20 mmol) of FA was dissolved in 3 mL of dried DMSO and added to a one neck flask. Next, 35.32 mg (0.22 mmol) CDI was added, and the reaction was stirred for one day at room temperature in the dark. 0.62 g (0.05 mmol) of F127 which has been previously dried overnight in vacuum, was added to the above solution. The reaction was allowed to proceed in the dark for 1 day at room temperature. The reaction mixture was transferred into a dialysis tube (Millipore, MWCO 1000) and dialyzed for 3 days against double deionized (DD) water, which was changed every 3–6 h. The final product was lyophilized and stored at −20 °C until use.

## 2.3 Preparation of BOSA loaded F127–FA NPs

A THF solution (1 mL) containing BOSA (changed from 0.5 to 4 mg) and F127–FA (fixed at 200 mg) was injected slowly into water (10 mL). And then the mixture was sonicated for 60 seconds. The suspension was then stirred at room temperature overnight to evaporate the organic solvent. After THF was evaporated, the solutions were filtered through 0.45 μm microfilter to collect the BOSA loaded F127–FA NPs suspension. NPAPF loaded F127–FA NPs were also prepared following the same procedure.

## 2.4 Preparation of BOSA–NPAPF co-loaded F127–FA NPs

A THF solution (1 mL) containing BOSA (changed from 0.5 to 4 mg), NPAPF (fixed at 2.7 mg) and F127–FA (fixed at 200 mg) was injected slowly into water (10 mL). And then the mixture was sonicated for 60 seconds. The suspension was then stirred at room temperature overnight to evaporate the organic solvent. After THF was evaporated, the solutions were filtered through 0.45 μm microfilter to collect the BOSA–NPAPF co-loaded F127–FA NPs suspension. BOSA–NPAPF co-loaded F127 NPs without surface folic acid were also prepared for comparative study following the same procedure.

## 2.5 Cell culture and imaging

MCF-7 breast cancer cells were cultured in folate-free Dulbecco's Modified Eagle's Medium (DMEM) supplemented with 10% fetal bovine serum, 1% penicillin streptomycin, and incubated at 37 °C in a 5% $CO_2$ atmosphere. Cells were seeded onto 35 mm coverglass bottom dishes and allowed to grow until a confluence of 80%. Prior to experiments, the medium was removed and the adherent cells were washed twice with PBS buffer to remove the remnant growth medium. The AIE fluorophores based NPs in FBS-free DMEM medium at 400 nM of NPAPF were then added to the plates, respectively. After incubation for 2 h, the cells were washed three times with PBS buffer and then fixed by 75% ethanol for 20 minutes, which were further washed twice with PBS buffer. The stained cells were subsequently used for bioimaging. Under a Nikon A1 confocal laser microscope system, the BOSA donor was excited at 405 nm and the emission of NPAPF acceptor was collected above 650 nm. No background fluorescence of cells was detected under the setting used.

### 2.6 Quantum yield measurements

Fluorescence quantum yield was measured using a Hitachi F4500 spectrofluorophotometer. Quinine sulfate ($\eta = 0.55$ in 1.0 N $H_2SO_4$, excitation wavelength of 365 nm) and fluorescein ($\eta =$ 0.79 in pH 11 solution, excitation wavelength of 492 nm) were used as standard to determine the fluorescence quantum yields of BOSA and NPAPF in solutions, respectively.[15a,b] Quantum yield, $\eta$ was calculated according to the following equation:[15c]

$$\eta_s = \eta_r \left(\frac{A_r}{A_s}\right)\left(\frac{I_s}{I_r}\right)\left(\frac{{n_s}^2}{{n_r}^2}\right) \quad (1)$$

where ($\eta_r$) and ($\eta_s$) are the fluorescence quantum yield of standards and the samples, respectively. $A_r$ and $A_s$ are the absorbance of the standards and the measured samples at the excitation wavelength, respectively. $I_r$ and $I_s$ are the integrated emission intensities of standards and the samples. $n_r$ and $n_s$ are the refractive indices of the corresponding solvents of the solutions, respectively. The final value of quantum yield was obtained from the average of four measurements with different absorbance in the range between 0.03 and 0.09. The standard deviation is less than 10%.

### 2.7 Cytotoxicity study

Cytotoxicity of the BOSA–NPAPF co-loaded F127–FA NPs against MCF-7 breast cancer cells was evaluated by MTT assay. MCF-7 breast cancer cells were seeded in 96-well plates ($4 \times 10^4$ cells per mL) and incubated for 24 h. Then, the BOSA–NPAPF co-loaded F127–FA NPs with the BOSA–NPAPF molar ratio of 1.5 : 1 in PBS buffers were added into the cell culture media to a final NPs concentration of 0.25 to 1 mg $mL^{-1}$ and the cells with the NPs were incubated in the 96 well plates at 37 °C. After the designated time intervals, the cells were washed twice with PBS buffer and then incubated in fresh medium (100 μL) and MTT solution (5 mg $mL^{-1}$, 10 μL) for another 3 h. 100 μL of DMSO were added into each well and the plate was gently shaken for 10 min at room temperature to dissolve the internalized purple formazan crystals. The absorbance was measured at a wavelength of 650 nm using a microplate reader (Thermo Varioskan Flash). Each experiment was conducted twice in triplicate. The result was expressed as a percentage of the absorbance of the blank control.

## 3 Results and discussion

### 3.1 Synthesis and characterization of AIE fluorophores loaded F127–FA NPs

Two AIE-active fluorophores, BOSA and NPAPF, were synthesized. BOSA is almost nonluminescent in tetrahydrofuran (THF) with an extremely low fluorescence quantum yield of 0.3%, whereas a suspension of BOSA in THF–water mixture (1 : 9 by volume) is highly emissive ($\eta$ = 30.2%), demonstrating the typical AIE feature of BOSA. NPAPF is also a strongly red fluorescent fluorophore and shows unique AIE characteristics. The two AIE fluorophores are completely insoluble in water, however, they could be dispersed into aqueous solution as fluorophore loaded NPs. Pluronic F127 (F127)[14] is selected as the polymer matrix for NP formulation in this study, which is widely used for drug delivery and bioimaging, with a typical polymeric structure of poly(ethylene oxide)-*block*-poly(propylene oxide)-*block*-poly(ethylene oxide) (PEO-PPO-PEO). Furthermore, by using F127–folic acid adduct (F127–FA) as the encapsulation matrix, the fluorescent NPs with good biocompatibility and surface folic acid functionalization were synthesized.

The AIE fluorophores loaded F127–FA NPs were synthesized through a modified desolvation method.[11] As shown in Scheme 1, a THF solution containing AIE fluorophores and F127–FA was injected slowly into water. And then the mixture was sonicated for 60 seconds. The suspension was obtained after THF evaporation under stirring overnight. After THF was evaporated, the solutions were filtered through 0.45 μm microfilter to collect the AIE fluorophores loaded F127–FA NPs suspension. During NP formation, the aggregation of AIE fluorophores and the hydrophobic PPO segments of F127–FA to afford the hydrophobic cores, however, the hydrophilic PEO segments as the shells of the NPs ensure the dispersion of NPs in water.

The average diameters of polymeric NPs with different BOSA or NPAPF concentrations were measured with dynamic light scattering (DLS) (ESI, Table S1†). The average diameters of BOSA loaded and NPAPF loaded F127 NPs are ranging from 20.5 to 25.6 nm and 21.8 to 26.2 nm, respectively. The average diameters of these NPs are influenced by the fluorophore concentrations. No apparent precipitates are observed in the dispersion, suggesting that the water-insoluble BOSA or NPAPF fluorophores are fully embedded in the hydrophobic interior of the self-assembled nanostructure of F127–FA.

To optimize the fluorescence emission through FRET, BOSA–NPAPF co-loaded F127–FA NPs with various donor–acceptor molar ratios were prepared. The concentration of NPAPF acceptor is set to be 400 nM, while the BOSA donor concentration is adjusted to modulate different donor–acceptor molar ratios. The average diameters of these NPs in aqueous solutions (determined by DLS) increase from 25.1 to 30.6 nm with the

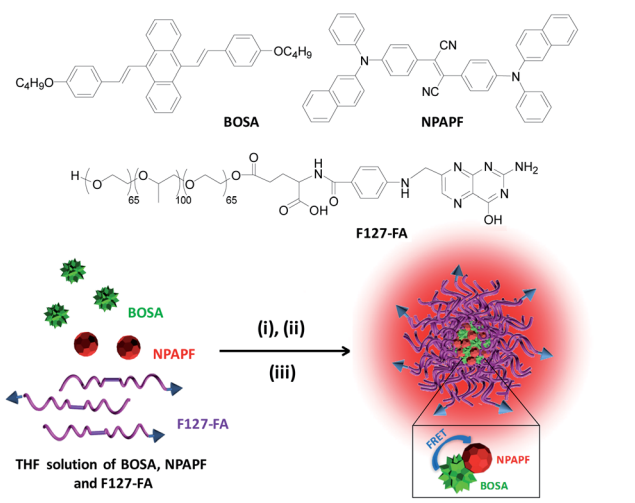


Scheme 1 Chemical structures of BOSA, NPAPF and F127–FA, and schematic illustration of the fabrication of BOSA–NPAPF co-loaded F127–FA NPs. (i) Mix with water; (ii) sonication; (iii) THF removal.

 

increase of molar ratio between BOSA and NPAPF from 0.25 : 1 to 1.5 : 1 (Table 1). As shown in Fig. 1, the volume average diameter of BOSA–NPAPF co-loaded F127–FA NPs with the BOSA–NPAPF molar ratio of 1.5 : 1 is 30.6 nm. The morphology of these NPs is investigated using transmission electron microscopy (TEM, Fig. 1 inset). The TEM image manifests that these NPs are spherical and can be distinguished as dark dots due to the high electron density of fluorophore molecules. The size of these NPs shows no obvious change after the NPs solutions were stored in dark at room temperature for 2 weeks. Such stability is desirable for use in biological applications.

### 3.2 Photophysical properties

Fig. 2 shows the emission spectra of BOSA in THF solution and BOSA loaded F127–FA NPs with different BOSA concentrations in aqueous solution. BOSA in THF solution emits very weakly, while the fluorescence intensity of BOSA loaded F127–FA NPs in aqueous solution is enhanced dramatically. In addition, the fluorescence intensity of BOSA aggregates increase with increasing BOSA concentration in NPs. When the BOSA concentration is increased to 0.4 mg $mL^{-1}$, the fluorescence intensity is ~84-fold higher than that in pure THF solution. The fluorescence intensity of NPAPF loaded F127–FA NPs in aqueous solution also increase with increasing NPAPF loading concentration (Fig. S1†). The significantly enhanced fluorescence intensity of AIE fluorophores loaded F127–FA NPs in aqueous solution compared to them in THF solution indicates restricted intramolecular rotation of AIE fluorophores in the NPs.[11]

Table 1 Properties of the BOSA–NPAPF co-loaded F127–FA NPs

| BOSA–NPAPF[a] | Size[b] [nm] | ET[c] [%] | Am[d] |
|---|---|---|---|
| 0.25 : 1 | 25.1 | >99 | 1.4 |
| 0.5 : 1 | 28.2 | >99 | 1.9 |
| 1 : 1 | 31.3 | 98.1 | 2.7 |
| 1.5 : 1 | 30.6 | 96.3 | 3.0 |

[a] Molar ratios of BOSA donor and NPAPF acceptor in F127–FA NPs. The concentration of NPAPF is 400 nM. [b] Average diameter of NPs determined by dynamic light scattering. [c] Energy-transfer efficiency of the BOSA by the NPAPF acceptor. [d] Amplification of the NPAPF by the BOSA donor.

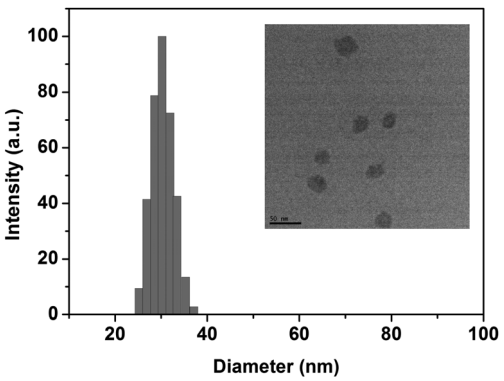


Fig. 1 Particle size distribution and morphological structure of BOSA–NPAPF co-loaded F127–FA Nps with the BOSA–NPAPF molar ratio of 1.5 : 1 studied by DLS and TEM (inset).

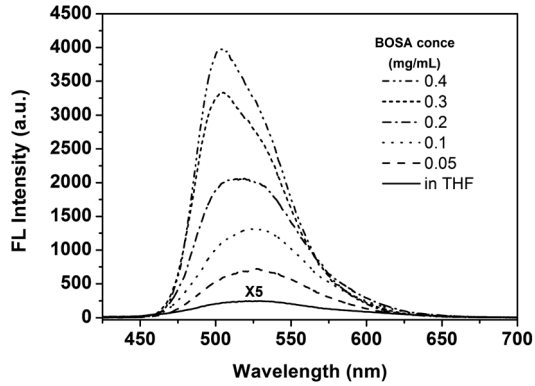


Fig. 2 Fluorescence emission spectra of BOSA in THF solution (0.4 mg $mL^{-1}$) and BOSA loaded F127–FA NPs with various BOSA loading concentrations.

Fig. 3 shows the absorption and emission spectra of individual BOSA and NPAPF loaded F127–FA NPs in aqueous solution. These BOSA loaded F127–FA NPs (0.4 mg $mL^{-1}$) in aqueous solution show an absorption maxima at 418 nm with an emission maximum at 503 nm. The maximum absorption peak of NPAPF loaded F127–FA NPs (0.4 mg $mL^{-1}$) is located at 500 nm. An important feature of Fig. 3 is that the emission spectrum of BOSA NPs overlaps well with the absorption spectrum of NPAPF NPs, suggesting that they are a reasonable donor–acceptor pair for FRET.

Fig. 4 shows the emission spectra of BOSA–NPAPF co-loaded F127–FA NPs with various BOSA–NPAPF molar ratio upon direct excitation at 405 nm. The concurrent incorporation of BOSA and NPAPF in the same NPs results in significant FRET process, which is characterized by the decrease in emission intensity of BOSA and simultaneous enhancement of fluorescence intensity of NPAPF. The molar ratio between BOSA and NPAPF were varied from 0.25 : 1 to 1.5 : 1 with a fixed NPAPF concentration of 400 nM. The FRET efficiency and amplification effect are also affected by the molecular ratios between BOSA and NPAPF (Table 1).

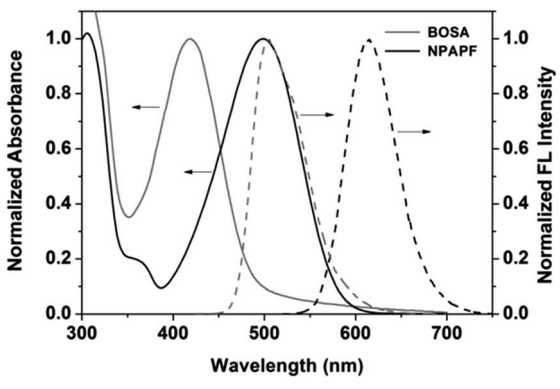


Fig. 3 Normalized UV-vis and fluorescence spectra of individual BOSA and NPAPF loaded F127–FA NPs in aqueous media.

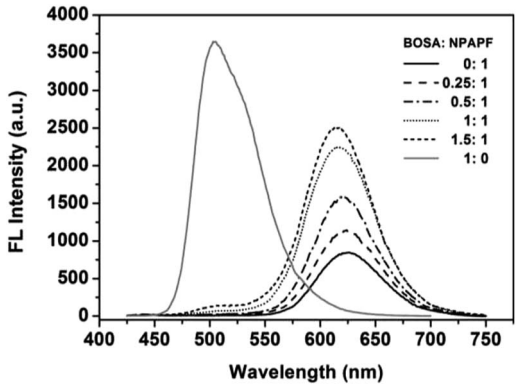


Fig. 4 Fluorescence spectra of BOSA–NPAPF co-loaded F127–FA NPs in aqueous solution.

The FRET efficiency is determined by studying the quenching of the BOSA donor fluorescence in the presence of the NPAPF acceptor. The amplification of emission from the NPAPF acceptor is calculated by comparing the fluorescence of NPAPF acceptor excited at 405 nm with and without BOSA donor. Higher than 99% of FRET efficiencies from BOSA to NPAPF is observed with the BOSA–NPAPF molar ratio of 0.5 : 1 indicating very complete energy transfer. The further increase of molar ratio between BOSA and NPAPF (1.5 : 1) results in 96.3% FRET efficiency. Under this condition, the emission of NPAPF could be amplified up to 3.0 folds. These results clearly indicate that the NPs core provides a good micro-reservoir environment to locate donor and acceptor molecules within the Förster distance (<10 nm) for efficient FRET.

### 3.3 Cellular imaging

The occurrence of FRET within BOSA–NPAPF co-loaded F127–FA NPs was investigated using confocal laser scanning microscopy (CLSM). For comparative study, the NPAPF loaded F127–FA NPs were also prepared for *in vitro* cellular imaging. In these experiments, MCF-7 breast cancer cells were incubated in culture medium with BOSA–NPAPF co-loaded F127–FA NPs and NPAPF loaded F127–FA NPs for 2 h containing 400 nM NPAPF, respectively. The images of Fig. 5 were taken by collecting the signals above 650 nm upon excitation at 405 nm. As shown in Fig. 5A, almost no fluorescence from the NPAPF loaded F127–FA NPs in the cytoplasm area of cells could be observed. However, comparing to the NPAPF loaded F127–FA NPs that show almost no fluorescence, a red fluorescence of BOSA–NPAPF co-loaded F127–FA NPs could be observed by the excitation with 405 nm light (Fig. 5C). The strong amplification of red fluorescence suggests efficient FRET from the BOSA donor to the NPAPF acceptor in the NPs. Moreover, the BOSA–NPAPF co-loaded F127–FA NPs show a large Stokes shift of ~245 nm, which can be used to improve the signal/background ratios of collected images by avoiding the autofluorescence of biosubstrate and interference between the excitation and emission.

In addition, the application of the BOSA–NPAPF co-loaded F127–FA NPs with FA functionalization for *in vitro* cellular

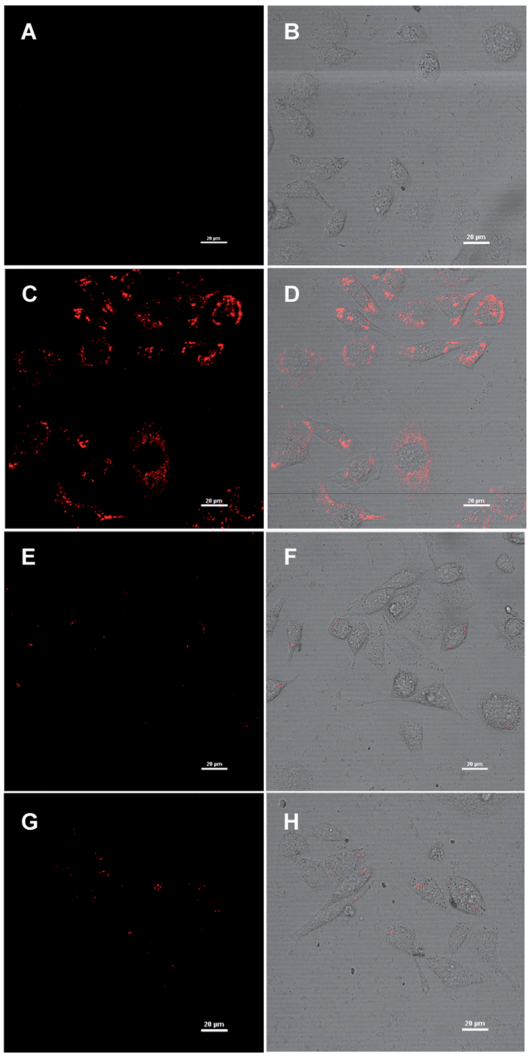


Fig. 5 CLSM images of MCF-7 breast cancer cells incubated with NPs: (A and B) are NPAPF loaded F127–FA NPs; (C and D) are BOSA–NPAPF co-loaded F127–FA NPs; (E and F) are BOSA–NPAPF co-loaded F127 NPs and (G and H) are MCF-7 cells incubated with free FA, then incubated with BOSA–NPAPF co-loaded F127–FA NPs. The fluorescence signal is collected above 650 nm upon excitation at 405 nm. Fluorescence images: (A, C, E and G); fluorescence/transmission overlay images: (B, D, F and H).

imaging was studied using CLSM. It is well known that targeted cell imaging is highly desirable for early stage cancer diagnosis. MCF-7 breast cancer cells were used as the target cells due to their have over-expressed FR on cell membranes.[16] Fig. 5C and E show the CLSM image of MCF-7 breast cancer cells after incubation with BOSA–NPAPF co-loaded F127–FA NPs and BOSA–NPAPF co-loaded F127 NPs without FA functionalization for 2 h, respectively. The higher fluorescence intensity observed in Fig. 5C as compared to that in Fig. 5E indicates that more BOSA–NPAPF co-loaded F127–FA NPs are internalized into MCF-7 breast cells *via* FR-mediated endocytosis.[17] To further demonstrate the specific labeling of these NPs to FR-overexpressed cells, we blocked FRs on MCF-7 cells by adding excessive free FA (0.04 mg $mL^{-1}$) prior to cell incubation with F127–FA NPs, only a

 

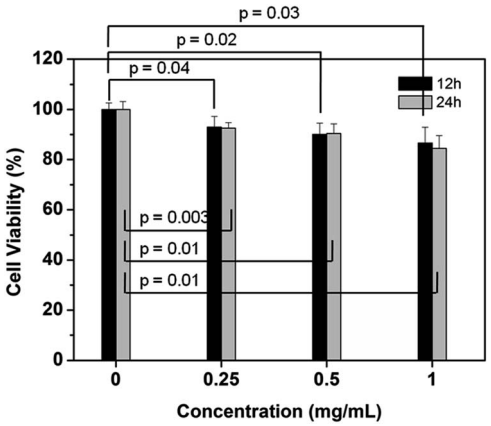


Fig. 6 Cell viability of MCF-7 breast cancer cells after incubation with BOSA–NPAPF co-loaded F127–FA NP suspensions at 0.25, 0.5 and 1 mg $mL^{-1}$ for 12 h and 24 h, respectively. Student's *t*-test was used for statistical analysis, $p < 0.05$.

few NPs were observed in the cytoplasm with a weak fluorescence (Fig. 5G). The free folate binding to FRs had hindered F127–FA NPs from attaching to the cell surface, thus hindered the internalization of these NPs.[12a]

### 3.4 Cytotoxicity evaluation using MTT assay

The cytotoxicity of the BOSA–NPAPF co-loaded F127–FA NPs with the BOSA–NPAPF molar ratio of 1.5 : 1 against MCF-7 breast cancer cells was investigated using a 3-(4,5-dimethylthiazol-2-yl)-2,5-diphenyltetrazolium bromide (MTT) cell-viability assay. Fig. 6 shows the cell viability after incubation with the NP suspensions at 0.25, 0.5, and 1 mg $mL^{-1}$ for 12 and 24 h, respectively. When MCF-7 cells were incubated with the NPs, low cytotoxicity with high cell viability (>90%) was measured after 24 h incubation with NPs concentration of 0.5 mg $mL^{-1}$. This observation suggests that these NPs may have potentials for *in vivo* applications.

## 4 Conclusions

In summary, we have developed a fluorescence-amplified AIE probe through incorporation of hydrophobic AIE fluorophores into biocompatible F127–FA NPs. By encapsulating both BOSA donor and NPAPF acceptor simultaneously within the NPs, a significant FRET effect was induced, which contributes to the notable increase of acceptor emission. Moreover, the BOSA–NPAPF co-loaded F127–FA NPs showed large Stokes shift, spherical morphology and low cytotoxicity. Application of these functionalized NPs for targeted cellular imaging were successfully demonstrated, showing bright fluorescence signals and specific targeting effect for FR-overexpressed cancer cells.

## Acknowledgements

We are grateful to the financial support from the Natural Science Foundation of China (20903072) and the National 973 Project (2013CB834702). Hongguang Lu is grateful for the support from 131 talents program of Tianjin.

## Notes and references

1 (*a*) J. H. Burroughes, D. D. C. Bradley, A. R. Brown, R. N. Marks, K. Mackay, R. H. Friend, P. L. Burns and A. B. Holmes, *Nature*, 1990, **347**, 539; (*b*) S. R. Forrest, *Nature*, 2004, **428**, 911; (*c*) X. Feng, L. Liu, S. Wang and D. Zhu, *Chem. Soc. Rev.*, 2010, **39**, 2411.

2 (*a*) X. Michalet, F. F. Pinaud, L. A. Bentolila, J. M. Tsay, S. Doose, J. J. Li, G. Sundaresan, A. M. Wu, S. S. Gambhir and S. Weiss, *Science*, 2005, **307**, 538; (*b*) P. Zrazhevskiy, M. Sena and X. H. Gao, *Chem. Soc. Rev.*, 2010, **39**, 4326; (*c*) J. Gao, K. Chen, R. Luong, D. M. Bouley, H. Mao, T. Qiao, S. S. Gambhir and Z. Cheng, *Nano Lett.*, 2011, **12**, 281.

3 (*a*) H. S. Choi, W. Liu, P. Misra, E. Tanaka, J. P. Zimmer, B. I. Ipe, M. G. Bawendi and J. V. Frangioni, *Nat. Biotech.*, 2007, **25**, 1165; (*b*) A. M. Smith, H. W. Duan, A. M. Mohs and S. M. Nie, *Adv. Drug Delivery Rev.*, 2008, **60**, 1226.

4 (*a*) W. C. Wu, C. Y. Chen, Y. Q. Tian, S. H. Jang, Y. N. Hong, Y. Liu, R. R. Hu, B. Z. Tang, Y. T. Lee, C. T. Chen, W. C. Chen and A. K. Y. Jen, *Adv. Funct. Mater.*, 2010, **20**, 1413; (*b*) A. M. Breul, M. D. Hager and U. S. Schubert, *Chem. Soc. Rev.*, 2013, **42**, 5366.

5 (*a*) S. W. Thomas, G. D. Joly and T. M. Swager, *Chem. Rev.*, 2007, **107**, 1339; (*b*) A. C. Grimsdale, K. L. Chan, R. E. Martin, P. G. Jokisz and A. B. Holmes, *Chem. Rev.*, 2009, **109**, 897.

6 (*a*) Y. N. Hong, J. W. Y. Lam and B. Z. Tang, *Chem. Commun.*, 2009, **29**, 4332; (*b*) Y. N. Hong, J. W. Y. Lam and B. Z. Tang, *Chem. Soc. Rev.*, 2011, **40**, 5361.

7 J. Luo, Z. Xie, J. W. Y. Lam, L. Cheng, H. Chen, C. Qiu, H. S. Kwok, X. Zhan, Y. Liu, D. Zhu and B. Z. Tang, *Chem. Commun.*, 2001, 1740.

8 (*a*) Y. Liu, C. Deng, L. Tang, A. Qin, R. Hu, J. Z. Sun and B. Z. Tang, *J. Am. Chem. Soc.*, 2011, **133**, 660; (*b*) J. L. Geng, K. Li, D. Ding, X. H. Zhang, W. Qin, J. Z. Liu, B. Z. Tang and B. Liu, *Small*, 2012, **8**, 3655; (*c*) S. Zhang, J. M. Yan, A. J. Qin, J. Z. Sun and B. Z. Tang, *Sci. China: Chem.*, 2013, **56**, 1253; (*d*) Q. Qi, X. Fang, Y. Liu, P. Zhou, Y. Zhang, B. Yang, W. Tian and S. X. Zhang, *RSC Adv.*, 2013, **3**, 16986; (*e*) X. Xue, Y. Zhao, L. Dai, X. Zhang, X. Hao, C. Zhang, S. Huo, J. Liu, C. Liu, A. Kumar, W. Chen, G. Zou and X. Liang, *Adv. Mater.*, 2014, **26**, 712.

9 (*a*) Z. Li, Y. Q. Dong, J. W. Lam, J. Sun, A. Qin, M. Häußler, Y. P. Dong, H. H. Sung, I. D. Williams, H. S. Kwok and B. Z. Tang, *Adv. Funct. Mater.*, 2009, **19**, 905; (*b*) Y. Yu, C. Feng, Y. Hong, J. Liu, S. Chen, K. M. Ng, K. Q. Luo and B. Z. Tang, *Adv. Mater.*, 2011, **23**, 3298; (*c*) H. B. Shi, J. Z. Liu, J. L. Geng, B. Z. Tang and B. Liu, *J. Am. Chem. Soc.*, 2012, **134**, 9569.

10 (*a*) J. T. He, B. Xu, F. P. Cheng, H. J. Xia, K. Li, L. Ye and W. Tian, *J. Phys. Chem. C*, 2009, **113**, 9892; (*b*) H. Lu, B. Xu, Y. Dong, F. Chen, Y. Li, Z. Li, J. He, H. Li and W. Tian, *Langmuir*, 2010, **26**, 6838; (*c*) Y. Dong, B. Xu, J. Zhang, X. Tan, L. Wang, J. Chen, H. Lu, S. Wen, B. Li, L. Ye, B. Zou and W. Tian, *Angew. Chem., Int. Ed.*, 2012, **51**, 10782.

11 (*a*) B. K. An, S. K. Kwon, S. D. Jung and S. Y. Park, *J. Am. Chem. Soc.*, 2002, **124**, 14410; (*b*) X. Y. Shen, W. Z. Yuan, Y. Liu, Q. Zhao, P. Lu, Y. Ma, I. D. Williams, A. Qin, J. Z. Sun and B. Z. Tang, *J. Phys. Chem. C*, 2012, **116**, 10541; (*c*) Z. F. Zhu, X. Y. Zhao, W. Qin, G. D. Chen, J. Qian and Z. P. Xu, *Sci. China: Chem.*, 2013, **56**, 1247.

12 (*a*) Y. L. Yang, F. F. An, Z. Liu, X. J. Zhang, M. J. Zhou, W. Li, X. J. Hao, C. S. Lee and X. H. Zhang, *Biomaterials*, 2012, **33**, 7803; (*b*) K. Li, W. Qin, D. Ding, N. Tomczak, J. L. Geng, R. Liu, J. Z. Liu, X. H. Zhang, H. W. Liu, B. Liu and B. Z. Tang, *Sci. Rep.*, 2013, **3**, 1150; (*c*) X. Zhang, X. Zhang, B. Yang, S. Wang, M. Liu, Y. Zhang, L. Tao and Y. Wei, *RSC Adv.*, 2013, **3**, 9633; (*d*) K. Li, D. Ding, Q. L. Zhao, J. Z. Sun, B. Z. Tang and B. Liu, *Sci. China: Chem.*, 2013, **56**, 1228; (*e*) D. Ding, J. Liang, H. Shi, R. T. K. Kwok, M. Gao, G. Feng, Y. Yuan, B. Z. Tang and B. Liu, *J. Mater. Chem. B*, 2014, **2**, 231; (*f*) X. Zhang, X. Zhang, B. Yang, M. Liu, W. Liu, Y. Chen and Y. Wei, *Polym. Chem.*, 2014, **5**, 399.

13 (*a*) H. Lu, F. Su, Q. Mei, X. Zhou, Y. Tian, W. Tian, R. H. Johnson and D. R. Meldrum, *J. Polym. Sci., Part A: Polym. Chem.*, 2012, **50**, 890; (*b*) H. Lu, F. Su, Q. Mei, Y. Tian, W. Tian, R. H. Johnson and D. R. Meldrum, *J. Mater. Chem.*, 2012, **22**, 9890.

14 (*a*) A. V. Kabanov, E. V. Batrakov and V. Y. Alakhov, *Adv. Drug Delivery Rev.*, 2002, **54**, 759; (*b*) J. Lin, J. Chen, S. Huang, J. Ko, Y. Wang, T. Chen and L. Wang, *Biomaterials*, 2009, **30**, 5114.

15 (*a*) J. N. Demas and G. A. Grosby, *J. Phys. Chem.*, 1971, **75**, 991; (*b*) S. Hamai and F. Hirayama, *J. Phys. Chem.*, 1983, **87**, 83; (*c*) H. S. Joshi, R. Jamshidi and Y. Tor, *Angew. Chem., Int. Ed*, 1999, **38**, 2721.

16 C. P. Leamon and J. A. Reddy, *Adv. Drug Delivery Rev.*, 2004, **56**, 1127.

17 (*a*) S. Gottschalk, R. J. Cristiano, L. C. Smith and S. L. C. Woo, *Gene Ther.*, 1994, **1**, 185; (*b*) P. S. Low, W. A. Henne and D. D. Doorneweerd, *Acc. Chem. Res.*, 2008, **41**, 120.

 